Quantitatively Tracking the Elevation of the Tibetan Plateau since the Cretaceous: Insights from Whole-rock Sr/Y and La/Yb Ratios

Fangyang Hu[1,2*], Fuyuan Wu[1,3,4], James B. Chapman[5], Mihai N. Ducea[2,6], Weiqiang Ji[1,4], Shuwen Liu[7]

[1]State Key Laboratory of Lithospheric Evolution, Institute of Geology and Geophysics, Chinese Academy of Sciences, Beijing 100029, PR China

[2]Department of Geosciences, University of Arizona, Tucson, AZ 85721, USA

[3]College of Earth and Planetary Sciences, University of Chinese Academy of Sciences, Beijing 100049, PR China

[4]Innovation Academy for Earth Science, Chinese Academy of Sciences, Beijing, 100029, PR China

[5]Department of Geology and Geophysics, University of Wyoming, Laramie, WY 82071, USA

[6]Faculty of Geology and Geophysics, University of Bucharest, Bucharest, Romania

[7]Key Laboratory of Orogenic Belts and Crustal Evolution, Ministry of Education, School of Earth and Space Sciences, Peking University, Beijing 100871, PR China

*Corresponding author: Fangyang Hu (hufangyang@mail.iggcas.ac.cn)

Key Points:

- Sr/Y and $(La/Yb)_N$ ratios of magmatic rocks can be used for estimating paleo-elevation of orogenic belts.
- Two proto-plateaus were formed successively during the Late Cretaceous in the central and southern Tibet before India-Asia collision.
- A paleo-valley formed during the Paleogene in central Tibet and the Tibetan Plateau reached present-day elevations during the Miocene.

Abstract

Crustal thickness, elevation, and Sr/Y and $(La/Yb)_N$ of magmatic rocks are strongly correlated for subduction-related and collision-related mountain belts. We quantitatively constrain the paleo-elevation of the Tibetan Plateau since the Cretaceous using empirically derived equations. The results are broadly consistent with previous estimates based on stable isotope and structural analyses, supporting a complex uplift history. Our data suggest that a proto-plateau formed in central Tibet during the Late Cretaceous and was higher than the contemporaneous Gangdese arc. This proto-plateau collapsed before the India-Asia collision, during the same time period that elevation in southern Tibet was increasing. During the India-Asia collision, northern and southern Tibet were uplifted first followed by renewed uplift in central Tibet, which suggests a more complicated uplift history than commonly believed. We contend that a broad paleo-valley formed during the Paleogene in central Tibet and that the whole Tibetan Plateau reached present-day elevations during the Miocene.

Plain Language Summary

Paleo-elevation is an important factor in understanding the mountain building processes. Strong correlations are observed between crustal thickness, elevation, and Sr/Y and $(La/Yb)_N$ of magmatic rocks for both subduction-related and collision-related mountain belts. We established empirical equations derived from modern examples and applied them to constrain the paleo-elevation evolution of the Tibetan Plateau since the Cretaceous. Our calculated results are broadly consistent with previous estimates based on stable isotope and structural analyses and document a complex uplift history. In the central Tibet, a proto-plateau with an elevation >3000 m was formed during the Late Cretaceous and was higher than the Gangdese continental arc in the south. This proto-plateau collapsed at the same time as the southern Tibet plateau (Lhasaplano) was uplifted prior to the India-Asia collision. formed before the India-Asia collision. During the India-Asia collision in the Cenozoic, northern and southern Tibet were uplift first, followed by uplift of central Tibet. A paleo-valley was formed in central Tibet during the Paleogene and elevations of the whole Tibetan Plateau similar to the present-day were achieved during the Miocene.

1 Introduction

The paleo-elevation history of the Tibetan Plateau (TP) remains a topic of intense debate (Botsyun et al., 2019; Deng et al., 2012, 2019; Deng & Ding, 2015; Ding et al., 2014, 2017; Ingalls et al., 2018; Quade et al., 2011; Rowley & Currie, 2006; Rowley & Garzione, 2007; Spicer et al., 2003; Su et al., 2019; Sun et al., 2015; Xu et al., 2013). Stable isotope (including clumped-isotope) studies proposed that the majority of the TP reached its present elevation during the Eocene (e.g., Ding et al., 2014; Ingalls et al., 2018; Rowley & Currie, 2006). However, paleontological studies questioned this viewpoint, suggesting that the TP did not achieve its present elevation until the Miocene (e.g., Deng et al., 2019; Deng & Ding, 2015; Su et al., 2019). Several models have been proposed for the Cenozoic uplift history of the TP, including synchronous uplift, northward stepwise uplift, incremental northward uplift, and differential uplift (England & Houseman, 1989; Law & Allen, 2020; Liu et al., 2016; Tapponnier et al., 2001). The pre-Cenozoic uplift history of the TP has only been described qualitatively and there is little information available outside of the Lhasa terrane (DeCelles et al., 2007; Kapp, DeCelles, Gehrels, et al., 2007; Lai, Hu, Garzanti, Sun, et al., 2019). The Gangdese arc region was thought to be at a relatively low elevation during the Early Cretaceous and become the Lhasaplano during the late Late Cretaceous to Paleocene (Ding et al., 2014; Kapp, DeCelles, Leier, et al., 2007). Another proto-plateau (Northern Lhasaplano) was proposed to be formed in the Northern and Central Lhasa terranes with a width > 160 km during the early Late Cretaceous (Lai, Hu, Garzanti, Sun, et al., 2019).

Most of the studies listed above use stable isotope (including clumped-isotope) or paleontological methods to estimate paleo-elevations (e.g., Spicer et al., 2003; Currie et al., 2005; Rowley and Garzione, 2007; Quade et al., 2011; Ding et al., 2017; Ingalls et al., 2018; Su et al., 2019; Deng et al., 2019). In recent years, additional methods have been developed to estimate Moho depth based on whole-rock geochemical and isotopic compositions of intermediate to felsic magmatic rocks (Alexander et al., 2019; Chapman et al., 2015; Chiaradia, 2015; F. Hu et al., 2017; Profeta et al., 2015), or the compositions of accessory minerals such as zircon (Balica et al., 2020; McKenzie et al., 2018). Since most convergent margins are in isostatic equilibrium at scales of hundreds of km, there is a direct correlation between crustal thickness and elevation assuming crustal Airy equilibrium (Airy, 1855; Lee et al., 2015), described as

$$dh/dH = (1 - \rho_c/\rho_m) \quad (1)$$

where h is the elevation, H is the crustal thickness, ρ_c is the crustal density, and ρ_m is the upper mantle density. Zhu et al. (2017) have estimated paleo-elevation for the southern Tibet using a two-step processes where they first calculated paleo-Moho depths using the equations of Profeta et al. (2015) then related those depths to paleo-elevation assuming Airy isostatic equilibrium (Eq. 1) with constant crustal and mantle densities. This contribution updates these previous studies by 1) directly establishing an empirical relation between elevation and Sr/Y and $(La/Yb)_N$ ratios of magmatic rocks, 2) exploring how variable crustal and mantle densities may affect paleo-elevation, and 3) expanding the analysis to central and northern Tibet. Reconstructing paleo-elevation changes for the TP since the Cretaceous suggests diachronous uplift and reveals a more dynamic uplift history than previously believed.

2 Methods

2.1 Empirical correlation equations

A global compilation of geochemical data of magmatic rocks from modern subduction zones and collisional zones and their corresponding elevations are presented in the Tables S1 and S2 in the supporting information. The data is organized into subsets based on location. Elevation for each data subset comes from the USGS National Elevation Dataset and NASA Shuttle Radar Topography Mission and was averaged after smoothing. Elevation uncertainty (1σ) is based on the standard deviation of individual sample location elevations within the data subsets. Moho depth is calculated based on the CRUST 1.0 model (http://igppweb.ucsd.edu/~gabi/rem.html), and referenced from Chapman et al. (2015), Profeta et al. (2015), and Hu et al. (2017) (Tables S3 and S4). A weighted least-squares regression between the elevation and Moho depth was established for subduction-related and collisional zones, respectively (Figure 1).

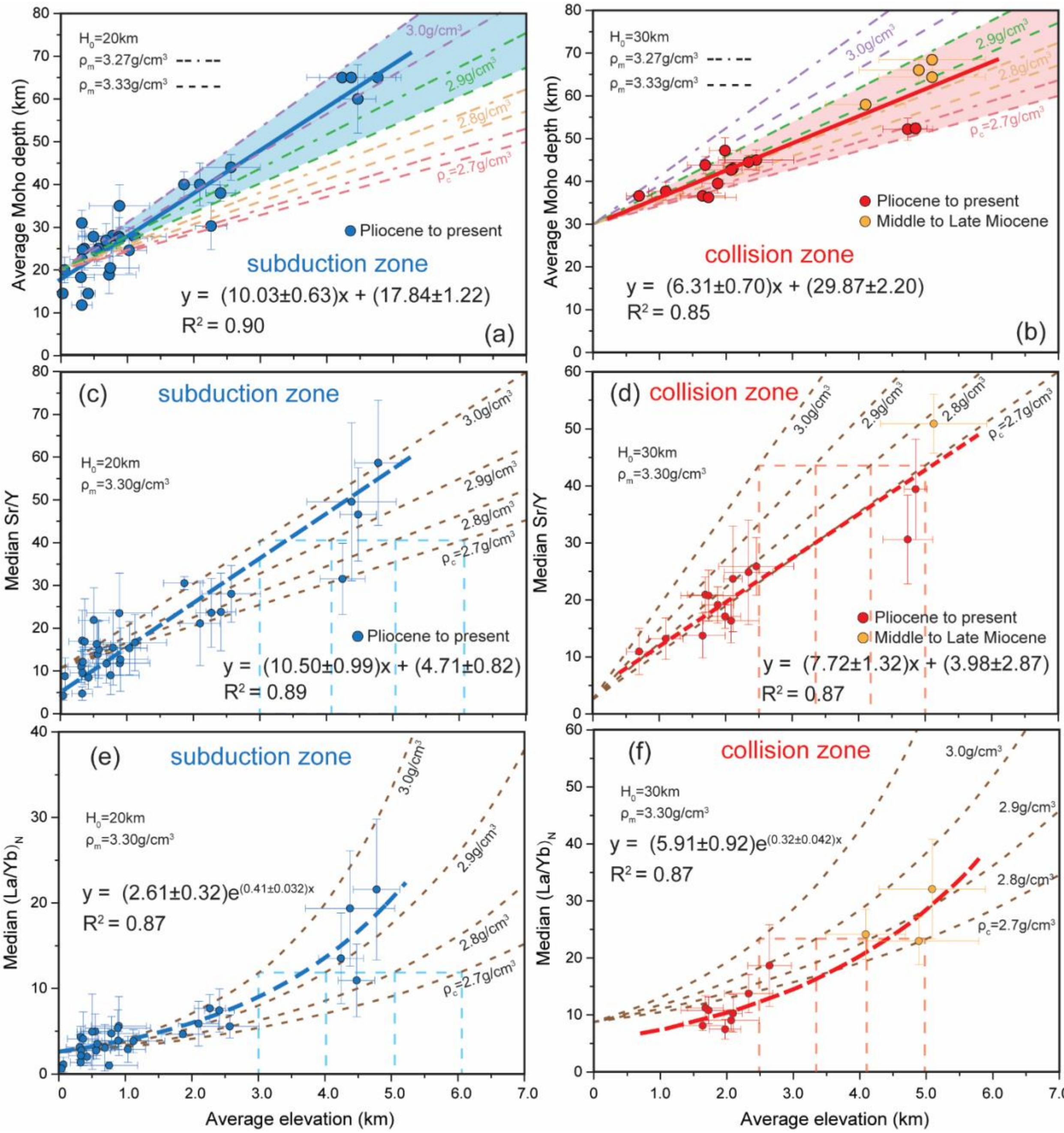

Figure 1. Global correlations between averaged elevations and average Moho depth, median Sr/Y and $(La/Yb)_N$ ratios from subduction zones (a, c and e) and collision zones (b, d and f). The blue circles represent the magmatic rocks from subduction zones formed during the Pliocene to present. The red (Pliocene to present) and orange circles (Middle to Late Miocene) represent magmatic rocks from collision zones. The brown dashed lines represent calculated reference lines based on the Airy isostasy and relationships between the Moho depth and median Sr/Y and $(La/Yb)_N$ (Chapman et al., 2015; F. Hu et al., 2017; Profeta et al., 2015). The given zero-elevation crustal thickness (H_0) and density of mantle (ρ_m) and crust (ρ_c) are shown on each diagram.

Geochemical data was filtered and processed using the methods of Chapman et al. (2015) and Hu et al. (2017) (Tables S3 and S4). Our data subsets include geochemical data from the

Pliocene to Quaternary age magmatic rocks for both subduction and collision zones. Miocene geochemical data from the TP are also included in our database because the Miocene paleo-elevation data is well-constrained and widely accepted (e.g., Currie et al., 2005; Quade et al., 2011; Rowley & Currie, 2006; Spicer et al., 2003). Samples from subduction zones with SiO_2 of 55–70 wt.%, MgO of 1.0–6.0 wt.%, and Rb/Sr ratio of 0.05–0.20 and samples from collision zones with SiO_2 of 55–72 wt.% and MgO of 0.5–6.0 wt.% were selected. Based on these criteria, we can efficiently removed those samples formed by partial melting or assimilation and fractional crystallization at shallow crustal level, which will result in the data having imprints of a thin crust (low elevation) but not the real crustal thickness (elevation) (Chapman et al., 2015; F. Hu et al., 2017). We then removed Sr/Y and $(La/Yb)_N$ outliers from each data subsets by using modified Thompson tau statistical method and calculated the median values of Sr/Y and $(La/Yb)_N$ and their standard deviations. We discarded data subsets with standard deviations higher than 10, except for those from the Andes. The data subsets from collision zones with average Rb/Sr higher than 0.35 were also rejected (F. Hu et al., 2017). The high La data subsets (>70 ppm) from collision zones were excluded from La/Yb compilation because the potential high temperature melting strongly elevates the La content but has little impact on Sr, Y and Yb contents, which leads to extremely high La/Yb ratios and their failure to constrain elevation (Figure S1).

We performed a weighted least-squares regression through these data subsets to obtain the correlation equations presented in Figure 1. Because we relate geochemical composition to elevation directly, no assumptions about variations in crustal and/or mantle densities are required. However, it is instructive to compare our empirically-derived paleo-elevation equations to models that relate $(La/Yb)_N$ ratio to paleo-elevation assuming Airy isostacy (e.g., Zhu et al., 2017). We explore a range of crustal and upper mantle densities based on the range of published P-/S-wave velocities and layer thicknesses for modern subduction and collisional orogenic systems (Figure S2; Table S5; Brocher, 2005). The transformation from P-/S-wave velocity to crustal density is based on the Nafe-Drake curve (Equation 2) and Brocher's regression fit (Equation 3) (Brocher, 2005), described as

$$\rho(g/cm^3) = 1.6612V_P - 0.4721V_P^2 + 0.0671V_P^3 - 0.0043V_P^4 + 0.000106V_P^5 \qquad (2)$$

$$V_P(km/s) = 0.9409 + 2.0947V_S - 0.8206V_S^2 + 0.2683V_S^3 - 0.0251V_S^4 \qquad (3)$$

where ρ is the crustal density, V_P is the P-wave velocity, V_S is the S-wave velocity. The upper mantle density refers to the values provided by He et al. (2014) and Lee et al. (2015).

2.2 The Tibetan Plateau

Geochemical data for Cretaceous to recent magmatic rocks in the TP were obtained from the Tibetan Magmatism Database (Table S6; Chapman and Kapp, 2017). Following previous authors (Yi et al., 2018; Zhu et al., 2019), we subdivided the Qiangtang and Lhasa terranes into five sub-terranes, including the Northern Qiangtang, Southern Qiangtang, Northern Lhasa, Central Lhasa, and Southern Lhasa terranes and investigate the paleo-elevation history of each separately (Figure 2). Because of the distinct tectonic settings of different terranes during different time periods, subduction-related and collision-related equations were applied for each terrane according to specific circumstances (see Table S7). Both methods were employed for comparison of magmatic rocks formed during the transition time form oceanic subduction to continental collision (e.g., ~120-100 Ma for the Southern Qiangtang and the Northern Lhasa terranes, and ~65-45 Ma for the Central and Southern Lhasa terranes). Paleo-elevation uncertainty is reported at the 2σ level and includes the uncertainty from the equation used and the standard deviation of Sr/Y or $(La/Yb)_N$ of each data subset.

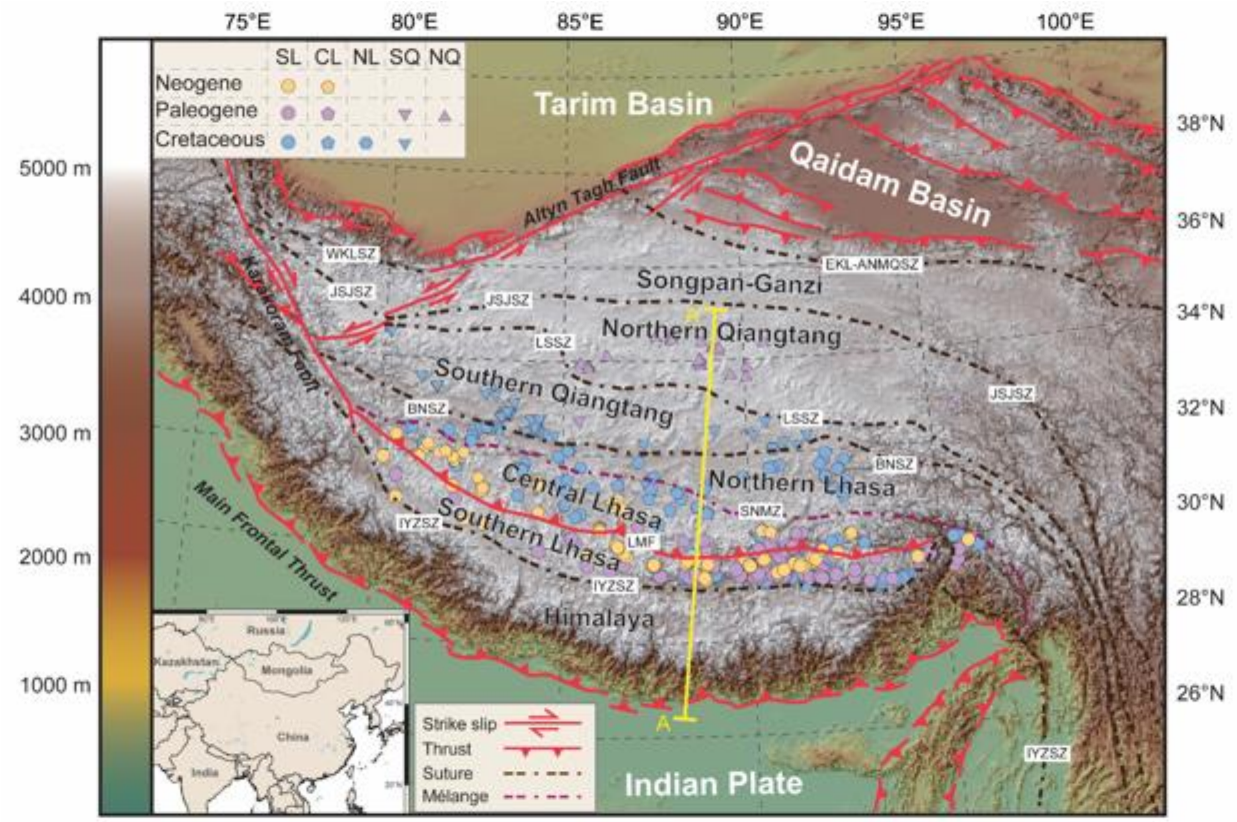

Figure 2. Digital elevation map of the TP showing the main active faults, suture zones, and terranes (after Taylor and Yin, 2009; Searle et al., 2016). The symbols represent locations and formation time of complied data. The abbreviations of main terranes are as follows: SL—Southern Lhasa; CL—Central Lhasa; NL—Northern Lhasa; SQ—Southern Qiangtang; NQ—Northern Qiangtang. The abbreviations of faults, mélange and suture zones separating the main terranes are as follows: EKL-ANMQSZ—Eastern Kunlun-Animaqing suture zone; JSJSZ—Jinshajiang suture zone; LSSZ—Longmuco-Shuanghu suture zone; BNSZ—Bangong-Nujiang suture zone; SNMZ—Shiquanhe-Nam Tso mélange zone; LMF—Luobadui-Milashan fault; IYZSZ—Indus-Yarlung Zangbo suture zone.

3 Results and Discussion

3.1 Empirical equations and their limitation

The empirical equations between the median Sr/Y and $(La/Yb)_N$ ratios of magmatic rocks and average elevations from subduction and collision zones are shown in Figure 1. The calculated regressions show good correlations with $R_2 > 0.85$. The empirical equations for subduction zones are as follows:

$$Sr/Y_S = (10.50 \pm 0.99) \times E + (4.71 \pm 0.82) \tag{4}$$

$$[(La/Yb)_N]_S = (2.61 \pm 0.32)e^{(0.41 \pm 0.032)E} \tag{5}$$

where E is the elevation in meters, and the subscript "S" means the subduction zone models. The empirical equations for collision zones are as follows:

$$Sr/Y_C = (7.72 \pm 1.32) \times E + (3.98 \pm 2.87) \tag{6}$$

$$[(La/Yb)_N]_C = (5.91 \pm 0.92)e^{(0.32 \pm 0.042)E} \tag{7}$$

where the subscript "C" refers to the collision zone models.

Based on the typical standard deviation of Sr/Y and $(La/Yb)_N$ in the data subsets and the uncertainty in our empirically-derived equations, the average uncertainty of this method is 500 to 1500 m (Figure S3). Paleo-elevation estimates higher than 6000 m for subduction systems [Sr/Y > 65; $(La/Yb)_N$ > 30] and collision zones [Sr/Y > 50; $(La/Yb)_N$ > 40] and lower than 1000 m [$(La/Yb)_N$ < 8] for collision zones are not considered valid because this range of values are not constrained by the data used to create the empirical relationships.

Strong correlations (R^2 > 0.85) between the elevation and Moho depth in modern subduction and collision zones confirms the effectiveness of equations 4-7 (Figure 1). The differences in equations for subduction zones and equations for collision zones are interpreted to be caused by the variations in crust and upper mantle density (Figure 1; Bassett et al., 2016; Lee et al., 2015). Previous studies that calculate paleo-elevation based on Airy isostasy and paleo-crustal thickness (e.g., Chapman et al., 2020; Zhu et al., 2017) implicitly assume that the crust and upper mantle density have not changed, which may not be valid for ancient orogens. Figure 1 shows how using different densities of the crust and upper mantle could influence estimates of paleo-elevation. The data suggest that choosing incorrect density values could result in paleo-elevation estimates up to 3000 m away from a true value (Figure 1 and S2). Therefore, our equations, which do not require assumption about density, could help reduce uncertainty. Figure 1 also makes predictions for the average crustal density in subduction and collisional systems based on our empirical equations, although this was not our primary goal. The predicted average crustal densities of ~2.8-3.0 g/cm^3 for subduction zones and ~2.6-2.8 g/cm^3 for collision zones are geologically realistic values and supports the utility of our new equations (Figure S2).

3.2 Paleo-elevation in the Tibetan Plateau since the Cretaceous

Our results are consistent with previous estimates based on stable isotopes (Figure 3; Tables S7 and S8; e.g., Currie et al., 2005; Ding et al., 2014; Ingalls et al., 2018; Xu et al., 2013). Results calculated from Sr/Y and $(La/Yb)_N$ generally overlap within uncertainty (Figure S4). When results calculated from both methods differ, the higher value was chosen to represent the elevation. This is because most lower values were calculated from $(La/Yb)_N$, which has a low resolution when the calculated elevation is lower than 3000 m (Figures. 1 and S4). The uncertainly of our calculation ranges from 300 m to 1500 m, with an average of ~900 m (Table S7).

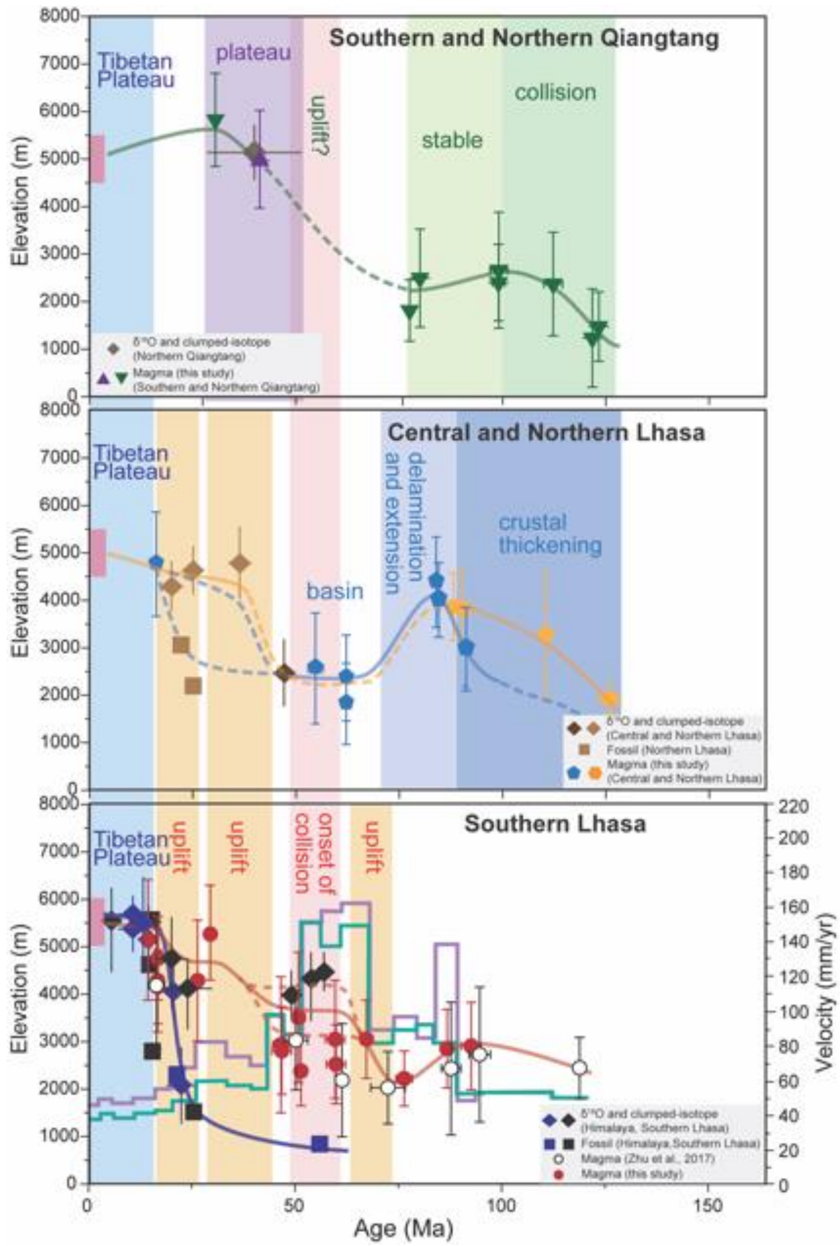

Figure 3. The elevation changes of different terranes of the TP since the Cretaceous (Table S7). Previous published elevation data based on isotopic and fossil studies are also shown for comparison (Table S8). Magmatic data from Zhu et al. (2017) were calculated using equations of this study. The purple and green jagged lines represent relative India-Asia convergence rate at eastern and western Himalayan syntaxis, respectively (after van Hinsbergen et al., 2011).

3.2.1 Early Cretaceous

All terranes in Tibet were located at relatively low elevation (≤ 2000 m) prior to the Cretaceous (Figures 3 and 4). During the Early Cretaceous, the Southern Qiangtang and Northern Lhasa terranes were uplifted from ~2000 m to 3000 m (Figure 3). At the same time, the paleo-elevation of the Southern Lhasa terrane (Gangdese arc) was relatively stable at ~2500 m (Figure 3).

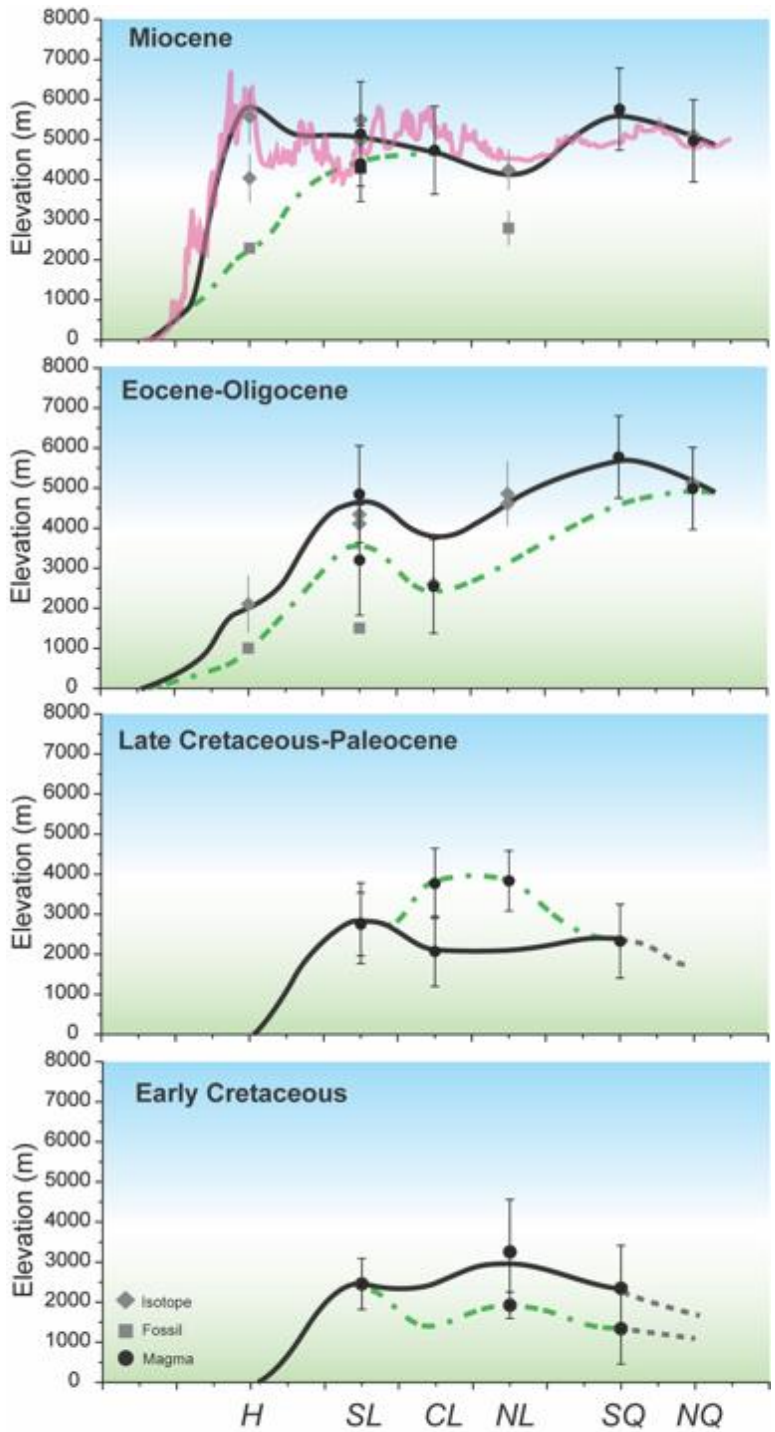

Figure 4. Proposed topography profile representing north (right) to south (left) transects of the TP from the Cretaceous to Miocene (Table S9). The transect location is illustrated as AA' in the Figure 2. The green dashed line represents the paleo-elevation during the middle Early Cretaceous, Late Cretaceous, Eocene, and early Miocene from bottom to top. The black solid line represents the paleo-elevation during the late Early Cretaceous, Paleocene, Oligocene, and late Miocene from bottom to top. The pink line represents the present elevation profile of the TP (AA' in Figure 1).

Our results from the South Qiangtang terrane are consistent with evidence for its fast exhumation during the Early Cretaceous and slow exhumation during ~90-60 Ma (Figure 3; Zhao et al., 2017, 2020). We interpret uplift of the Southern Qiangtang terrane to be related to the collision between the Qiangtang and Lhasa terrane along the Bangong-Nujiang suture in the Early Cretaceous (Kapp, DeCelles, Gehrels, et al., 2007; Lai, Hu, Garzanti, Xu, et al., 2019; Zhao et al., 2020). The low elevations in the Northern and Central Lhasa terranes during the initial collision period are consistent with the contemporaneous carbonate deposition (Lai, Hu, Garzanti, Xu, et al., 2019). As collision continued, the elevation of the Northern Lhasa terrane increased to ~3000 m during the Early Cretaceous (Figures 3 and 4). No change in the elevation of the Southern Lhasa terrane during the Early Cretaceous is consistent with the fore-arc sedimentary records and a constant convergence rate between India and Asia (J.-G. Wang et al., 2020).

3.2.2 Late Cretaceous

During the early Late Cretaceous, the Northern Lhasa and Central Lhasa terranes increased in elevation to ~4000 m (Figure 3). Based on these results, we interpret the existence of a proto-plateau (>3000 m; the Northern Lhasaplano) in central Tibet during the Late Cretaceous, which exceeded the elevation of the Southern Qiangtang terrane (Figure 4). Opposite to the Central and Northern Lhasa terranes, the paleo-elevation of the Southern Lhasa terrane (Gangdese arc) decreased to ~2000 m at ca. 75 Ma (Figure 3).

Earlier uplift of the Northern Lhasa terrane relative to the Central Lhasa terrane is corroborated by sedimentological studies (DeCelles et al., 2007; Kapp, DeCelles, Gehrels, et al., 2007; Lai, Hu, Garzanti, Sun, et al., 2019), and paleocurrent data supports a higher elevation of the Lhasa terrane relative to the Qiangtang terrane during this stage (Figure 4; Lai, Hu, Garzanti, Sun, et al., 2019). The high elevation was reflected by a thickened crust during the early Late Cretaceous, evidenced by lower-crustal derived adakitic rocks (G.-Y. Sun et al., 2015; Yi et al., 2018). Tectonic shortening/thrusting also indicates the upper crust was thickened significantly during the Late Cretaceous (DeCelles et al., 2007; Kapp, DeCelles, Gehrels, et al., 2007), which supports the concept of the Northern Lhasaplano (Figure 4; Lai, Hu, Garzanti, Sun, et al., 2019; Murphy et al., 1997; J.-G. Wang et al., 2020). The initial uplift of the Gangdese arc during ~96-90 Ma is consistent with increasing input of volcanic rocks from the Gangdese arc to the retro-arc basin (J.-G. Wang et al., 2020). Acceleration of the convergence rate at ~90 Ma may have also resulted increased shortening, crustal thickening, and uplift (Figure 3; S. Li, van Hinsbergen, Shen, et al., 2020). Slab rollback and lower crustal delamination has been proposed for the Gangdese arc (Ji et al., 2014; Zhu et al., 2017), which may explain the subsequent decrease in paleo-elevation observed there and may also lower the elevation in the Central and Northern Lhasa terranes (Figure 3).

3.2.3 Paleocene

The elevation of the Northern Lhasaplano in central Tibet decreased to ~2500 m at the Paleocene (Figure 3; Xu et al., 2015). Conversely, the Southern Lhasa paleo-elevation increased to ~3000 m by the start of the Paleogene, which is interpreted to mark the birth of the Lhasaplano. The Southern Lhasa terrane maintained an elevation of ~3000-3500 m throughout the Paleocene (Figure 3). Therefore, two proto-plateaus were formed successively during the Late Cretaceous to Early Paleogene in the central and southern Tibet, respectively (Figure 4).

The low elevation in central Tibet during this time may be related to pervious post-collisional extension and delamination of the lower crust (Meng et al., 2014; Yi et al., 2018). Increasing elevation in the Southern Lhasa terrane is consistent with evidence for crustal thickening and ongoing subduction (Figure 3; Kapp, DeCelles, Leier, et al., 2007; Zhu et al., 2017). Deformation of the Shexing Formation and unconformities during ~75-65 Ma in the Southern Lhasa documented this crust thickening and uplift process (Leier et al., 2007). The striking increase of the convergence rate at ~70 Ma may also connect to the uplift in the Southern Lhasa (Figure 3; S. Li, van Hinsbergen, Najman, et al., 2020).

3.2.4 Eocene-Oligocene

During the Eocene to Oligocene, the Qiangtang terrane increased in elevation to ~5000 m (Figure 3). In contrast, the Southern Lhasa terrane kept an elevation of ~3000-3500 m during the Early Eocene and was uplifted significantly during the Late Eocene to Oligocene reaching ~4000-5000 m (Figure 3). However, the Central Lhasa terrane and possibly the Northern Lhasa terrane maintained a low elevation of ca. 2500 m during the Eocene, which we interpret to represent a paleo-valley between high elevations to the north in the Qiangtang terrane and to the south in the Southern Lhasa terrane (Figures 3 and 4).

Uplift of the Qiangtang block is consistent with evidence for major crustal shortening and rapid exhumation (Figure 3; Kapp, DeCelles, Gehrels, et al., 2007; Rohrmann et al., 2012; C. Wang et al., 2008; Z. Zhao et al., 2020). Magnetic susceptibility analysis of the Gonjo Basin suggests tectonic shortening in the Qiangtang terrane during ~52-48 Ma (S. Li, van Hinsbergen, Shen, et al., 2020), and oxygen isotopic data suggest that the Qiangtang terrane experienced a significant uplift event during the Eocene to Oligocene (Xu et al., 2013). Our elevation estimates for the Southern Lhasa terrane during the Early Eocene are slightly lower than those from the isotopic studies (~4000-4500 m) (e.g. Ding et al., 2014), although they are consistent within uncertainty (Figure 3). The initial India-Asia collision and deceleration of convergence at ~55 Ma should have contributed to crustal deformation (X. Hu et al., 2016; Zheng & Wu, 2018). However, the calculated results show no obvious change of paleo-elevation in the Southern Lhasa terrane, which could be related to a contemporaneous increase in erosion (Ding et al., 2014; Xu et al., 2015). Upper crustal shortening of the Central Lhasa terrane was low during ~50-30 Ma (Kapp, DeCelles, Gehrels, et al., 2007), supporting our interpretation of a paleo-valley. Isotopic and paleontological data also support the presence of a paleo-valley or intermontane basin (Nima-Lunpola Basin) (Figure 4; Ding et al., 2014; Su et al., 2019). Paleontological and paleoclimatological data show that this valley existed as a topographic feature until the Oligocene (Botsyun et al., 2019; Su et al., 2019; B. Sun et al., 2015), but isotopic data suggests its uplift during the Late Eocene (Rowley & Currie, 2006). The deceleration of convergence at ~45 Ma is proposed to be related to the break-off of the subducted slab (Ji et al., 2016). After this, the long-term low velocity of convergence rate supports a continuous hard collision between India and Asia (van Hinsbergen et al., 2011). Uplift of the Southern Lhasa during the Late Eocene to Oligocene is consistent with rapid exhumation of the Gangdese arc and the activating of the Gangdese thrust belt (~30-23 Ma) (Kapp, DeCelles, Gehrels, et al., 2007; Y. Li et al., 2015; Yin et al., 1999). Late Oligocene to Miocene post-collisional adakitic rocks in southern Tibet also supports thick crust during that time (Chung et al., 2005; Hou et al., 2012).

3.2.5 Miocene

During the Miocene, the convergence rate between India and Asia continued to slow and the Southern Lhasa and Himalaya terranes continued to be uplifted (Figure 3). Underthrusting of India beneath the TP resulted in the expansion of the Himalayan thrust belt and its extraordinarily rapid uplift (Ding et al., 2017; Gébelin et al., 2013; Y. Li et al., 2015). The rise of the Himalaya marked the final formation of the TP (Figure 4; Currie et al., 2005; D.B. Rowley & Currie, 2006).

4 Conclusions

Empirically-derived equations are presented relating Sr/Y and $(La/Yb)_N$ of intermediate igneous rocks to elevation. These equations can be effectively used to reconstruct the paleo-elevation histories for ancient orogens. Our calculated results for the TP are consistent with results from other paleoaltimetry studies and geological evidence. The Cretaceous amalgamation between the Lhasa and Qiangtang terranes helped to build a proto-plateau >3000 m in elevation in central Tibet, which exceeded the paleo-elevation of the Gangdese arc during the same time. Orogenic collapse reshaped the topography of the central Tibet by the end of the Cretaceous. The TP experienced a differential uplift history during the India-Asia collision. The early uplift of the Qiangtang and Southern Lhasa terranes formed a broad paleo-valley in central Tibet during the Eocene before present-day elevations of the whole TP were achieved during the Miocene.

Acknowledgments

F.Y.H and F.Y.W acknowledge support from National Natural Science Foundation of China [41888101, 41902055] and China Postdoctoral Science Foundation [2018M640177]. M.N.D. acknowledges support from US National Science Foundation [EAR-1725002] and the Romanian Executive Agency for Higher Education, Research, Development and Innovation Funding project [PN-III-P4-ID-PCCF-2016-0014]. The authors declare no conflict of interest. All the data for this research are available online (https://doi.org/10.6084/m9.figshare.12457376.v2) and in the supporting information.

References

Airy, G. B. (1855). On the computation of the effect of the attraction of mountain-masses, as disturbing the apparent astronomical lattitude of stations in geodetic surveys. *Royal Society*, *145*, 101–103. https://doi.org/doi.org/10.1098/rstl.1855.0003

Alexander, E. W., Wielicki, M. M., Harrison, T. M., DePaolo, D. J., Zhao, Z. D., & Zhu, D. C. (2019). Hf and Nd Isotopic Constraints on Pre- and Syn-collisional Crustal Thickness of Southern Tibet. *Journal of Geophysical Research: Solid Earth*, *124*(11), 11038–11054. https://doi.org/10.1029/2019JB017696

Balica, C., Ducea, M. N., Gehrels, G. E., Kirk, J., Roban, R. D., Luffi, P., et al. (2020). A zircon petrochronologic view on granitoids and continental evolution. *Earth and Planetary Science Letters*, *531*, 116005. https://doi.org/10.1016/j.epsl.2019.116005

Bassett, D., Kopp, H., Sutherland, R., Henrys, S., Watts, A. B., Timm, C., et al. (2016). Crustal structure of the Kermadec arc from MANGO seismic refraction profiles: Kermadec Arc Crustal Structure. *Journal of Geophysical Research: Solid Earth*, *121*(10), 7514–7546. https://doi.org/10.1002/2016JB013194

Botsyun, S., Sepulchre, P., Donnadieu, Y., Risi, C., Licht, A., & Caves Rugenstein, J. K. (2019). Revised paleoaltimetry data show low Tibetan Plateau elevation during the Eocene. *Science*, *363*(6430), eaaq1436. https://doi.org/10.1126/science.aaq1436

Brocher, T. M. (2005). Empirical Relations between Elastic Wavespeeds and Density in the Earth's Crust. *Bulletin of the Seismological Society of America*, *95*(6), 2081–2092. https://doi.org/10.1785/0120050077

Chapman, J. B., & Kapp, P. (2017). Tibetan Magmatism Database. *Geochemistry, Geophysics, Geosystems*, *18*(11), 4229–4234. https://doi.org/10.1002/2017GC007217

Chapman, J. B., Ducea, M. N., DeCelles, P. G., & Profeta, L. (2015). Tracking changes in crustal thickness during orogenic evolution with Sr/Y: An example from the North American Cordillera. *Geology*, *43*(10), 919–922. https://doi.org/10.1130/g36996.1

Chapman, J. B., Greig, R., & Haxel, G. B. (2020). Geochemical evidence for an orogenic plateau in the southern U.S. and northern Mexican Cordillera during the Laramide orogeny. *Geology*, *48*(2), 164–168. https://doi.org/10.1130/G47117.1

Chiaradia, M. (2015). Crustal thickness control on Sr/Y signatures of recent arc magmas: an Earth scale perspective. *Sci Rep*, *5*, 8115. https://doi.org/10.1038/srep08115

Chung, S.-L., Chu, M.-F., Zhang, Y., Xie, Y., Lo, C.-H., Lee, T.-Y., et al. (2005). Tibetan tectonic evolution inferred from spatial and temporal variations in post-collisional magmatism. *Earth-Science Reviews*, *68*(3–4), 173–196. https://doi.org/10.1016/j.earscirev.2004.05.001

Currie, B. S., Rowley, D. B., & Tabor, N. J. (2005). Middle Miocene paleoaltimetry of southern Tibet: Implications for the role of mantle thickening and delamination in the Himalayan orogen. *Geology*, *33*(3), 181–184. https://doi.org/10.1130/g21170.1

DeCelles, P. G., Kapp, P., Ding, L., & Gehrels, G. E. (2007). Late Cretaceous to middle Tertiary basin evolution in the central Tibetan Plateau: Changing environments in response to tectonic partitioning, aridification, and regional elevation gain. *GSA Bulletin*, *119*(5–6), 654–680. https://doi.org/10.1130/B26074.1

Deng, T., & Ding, L. (2015). Paleoaltimetry reconstructions of the Tibetan Plateau: progress and contradictions. *National Science Review*, *2*(4), 417–437. https://doi.org/10.1093/nsr/nwv062

Deng, T., Li, Q., Tseng, Z. J., Takeuchi, G. T., Wang, Y., Xie, G., et al. (2012). Locomotive implication of a Pliocene three-toed horse skeleton from Tibet and its paleo-altimetry significance. *Proceedings of the National Academy of Sciences*, *109*(19), 7374–7378. https://doi.org/10.1073/pnas.1201052109

Deng, T., Wang, X., Wu, F., Wang, Y., Li, Q., Wang, S., & Hou, S. (2019). Review: Implications of vertebrate fossils for paleo-elevations of the Tibetan Plateau. *Global and Planetary Change*, *174*, 58–69. https://doi.org/10.1016/j.gloplacha.2019.01.005

Ding, L., Xu, Q., Yue, Y., Wang, H., Cai, F., & Li, S. (2014). The Andean-type Gangdese Mountains: Paleoelevation record from the Paleocene–Eocene Linzhou Basin. *Earth and Planetary Science Letters*, *392*, 250–264. https://doi.org/10.1016/j.epsl.2014.01.045

Ding, L., Spicer, R. A., Yang, J., Xu, Q., Cai, F., Li, S., et al. (2017). Quantifying the rise of the Himalaya orogen and implications for the South Asian monsoon. *Geology*, *45*(3), 215–218. https://doi.org/10.1130/G38583.1

England, P., & Houseman, G. (1989). Extension during continental convergence, with application to the Tibetan Plateau. *Journal of Geophysical Research: Solid Earth*, *94*(B12), 17561–17579. https://doi.org/10.1029/JB094iB12p17561

Gébelin, A., Mulch, A., Teyssier, C., Jessup, M. J., Law, R. D., & Brunel, M. (2013). The Miocene elevation of Mount Everest. *Geology*, *41*(7), 799–802. https://doi.org/10.1130/G34331.1

He, R., Liu, G., Golos, E., Gao, R., & Zheng, H. (2014). Isostatic gravity anomaly, lithospheric scale density structure of the northern Tibetan plateau and geodynamic causes for potassic lava eruption in Neogene. *Tectonophysics*, *628*, 218–227. https://doi.org/10.1016/j.tecto.2014.04.047

Hou, Z.-Q., Zheng, Y.-C., Zeng, L.-S., Gao, L.-E., Huang, K.-X., Li, W., et al. (2012). Eocene–Oligocene granitoids in southern Tibet: Constraints on crustal anatexis and tectonic evolution of the Himalayan orogen. *Earth and Planetary Science Letters*, *349–350*, 38–52. https://doi.org/10.1016/j.epsl.2012.06.030

Hu, F., Ducea, M. N., Liu, S., & Chapman, J. B. (2017). Quantifying Crustal Thickness in Continental Collisional Belts: Global Perspective and a Geologic Application. *Sci Rep*, *7*(1), 7058. https://doi.org/10.1038/s41598-017-07849-7

Hu, X., Garzanti, E., Wang, J., Huang, W., An, W., & Webb, A. (2016). The timing of India-Asia collision onset – Facts, theories, controversies. *Earth-Science Reviews*, *160*, 264–299. https://doi.org/10.1016/j.earscirev.2016.07.014

Ingalls, M., Rowley, D., Olack, G., Currie, B., Li, S., Schmidt, J., et al. (2018). Paleocene to Pliocene low-latitude, high-elevation basins of southern Tibet: Implications for tectonic models of India-Asia collision, Cenozoic climate, and geochemical weathering. *GSA Bulletin*, *130*(1–2), 307–330. https://doi.org/10.1130/B31723.1

Ji, W.-Q., Wu, F.-Y., Chung, S.-L., & Liu, C.-Z. (2014). The Gangdese magmatic constraints on a latest Cretaceous lithospheric delamination of the Lhasa terrane, southern Tibet. *Lithos*, *210–211*, 168–180. https://doi.org/10.1016/j.lithos.2014.10.001

Ji, W.-Q., Wu, F.-Y., Chung, S.-L., Wang, X.-C., Liu, C.-Z., Li, Q.-L., et al. (2016). Eocene Neo-Tethyan slab breakoff constrained by 45 Ma oceanic island basalt–type magmatism in southern Tibet. *Geology*, *44*(4), 283–286. https://doi.org/10.1130/G37612.1

Kapp, P., DeCelles, P. G., Gehrels, G. E., Heizler, M., & Ding, L. (2007). Geological records of the Lhasa-Qiangtang and Indo-Asian collisions in the Nima area of central Tibet. *Geological Society of America Bulletin*, *119*(7–8), 917–933. https://doi.org/10.1130/B26033.1

Kapp, P., DeCelles, P. G., Leier, A. L., Fabijanic, J. M., He, S., Pullen, A., et al. (2007). The Gangdese retroarc thrust belt revealed. *GSA Today*, *17*(7), 4. https://doi.org/10.1130/GSAT01707A.1

Lai, W., Hu, X., Garzanti, E., Xu, Y., Ma, A., & Li, W. (2019). Early Cretaceous sedimentary evolution of the northern Lhasa terrane and the timing of initial Lhasa-Qiangtang collision. *Gondwana Research*, *73*, 136–152. https://doi.org/10.1016/j.gr.2019.03.016

Lai, W., Hu, X., Garzanti, E., Sun, G., Garzione, C. N., BouDagher-Fadel, M., & Ma, A. (2019). Initial growth of the Northern Lhasaplano, Tibetan Plateau in the early Late Cretaceous (ca. 92 Ma). *GSA Bulletin*. https://doi.org/10.1130/B35124.1

Law, R., & Allen, M. B. (2020). Diachronous Tibetan Plateau landscape evolution derived from lava field geomorphology. *Geology*. https://doi.org/10.1130/G47196.1

Lee, C.-T. A., Thurner, S., Paterson, S., & Cao, W. (2015). The rise and fall of continental arcs: Interplays between magmatism, uplift, weathering, and climate. *Earth and Planetary Science Letters*, *425*, 105–119. https://doi.org/10.1016/j.epsl.2015.05.045

Leier, A. L., DeCelles, P. G., Kapp, P., & Ding, L. (2007). The Takena Formation of the Lhasa terrane, southern Tibet: The record of a Late Cretaceous retroarc foreland basin. *GSA Bulletin*, *119*(1–2), 31–48. https://doi.org/10.1130/B25974.1

Li, S., van Hinsbergen, D. J. J., Shen, Z., Najman, Y., Deng, C., & Zhu, R. (2020). Anisotropy of Magnetic Susceptibility (AMS) Analysis of the Gonjo Basin as an Independent Constraint to Date Tibetan Shortening Pulses. *Geophysical Research Letters*, *47*(8), e2020GL087531. https://doi.org/10.1029/2020GL087531

Li, S., van Hinsbergen, D. J. J., Najman, Y., Liu-Zeng, J., Deng, C., & Zhu, R. (2020). Does pulsed Tibetan deformation correlate with Indian plate motion changes? *Earth and Planetary Science Letters*, *536*, 116144. https://doi.org/10.1016/j.epsl.2020.116144

Li, Y., Wang, C., Dai, J., Xu, G., Hou, Y., & Li, X. (2015). Propagation of the deformation and growth of the Tibetan–Himalayan orogen: A review. *Earth-Science Reviews*, *143*, 36–61. https://doi.org/10.1016/j.earscirev.2015.01.001

Liu, X., Xu, Q., & Ding, L. (2016). Differential surface uplift: Cenozoic paleoelevation history of the Tibetan Plateau. *Science China Earth Sciences*, *59*(11), 2105–2120. https://doi.org/10.1007/s11430-015-5486-y

McKenzie, N. R., Smye, A. J., Hegde, V. S., & Stockli, D. F. (2018). Continental growth histories revealed by detrital zircon trace elements: A case study from India. *Geology*, *46*(3), 275–278. https://doi.org/10.1130/G39973.1

Meng, F.-Y., Zhao, Z., Zhu, D.-C., Mo, X., Guan, Q., Huang, Y., et al. (2014). Late Cretaceous magmatism in Mamba area, central Lhasa subterrane: Products of back-arc extension of Neo-Tethyan Ocean? *Gondwana Research*, *26*(2), 505–520. https://doi.org/10.1016/j.gr.2013.07.017

Murphy, M. A., Yin, A., Harrison, T. M., Dürr, S. B., Z, C., Ryerson, F. J., et al. (1997). Did the Indo-Asian collision alone create the Tibetan plateau? *Geology*, *25*(8), 719–722. https://doi.org/10.1130/0091-7613(1997)025<0719:DTIACA>2.3.CO;2

Profeta, L., Ducea, M. N., Chapman, J. B., Paterson, S. R., Gonzales, S. M., Kirsch, M., et al. (2015). Quantifying crustal thickness over time in magmatic arcs. *Sci Rep*, *5*, 17786. https://doi.org/10.1038/srep17786

Quade, J., Breecker, D. O., Daëron, M., & Eiler, J. (2011). The paleoaltimetry of Tibet: An isotopic perspective. *American Journal of Science*, *311*(2), 77–115. https://doi.org/10.2475/02.2011.01

Rohrmann, A., Kapp, P., Carrapa, B., Reiners, P. W., Guynn, J., Ding, L., & Heizler, M. (2012). Thermochronologic evidence for plateau formation in central Tibet by 45 Ma. *Geology*, *40*(2), 187–190. https://doi.org/10.1130/G32530.1

Rowley, D. B., & Currie, B. S. (2006). Palaeo-altimetry of the late Eocene to Miocene Lunpola basin, central Tibet. *Nature*, *439*, 677–681. https://doi.org/10.1038/nature04506

Rowley, D. B., & Garzione, C. N. (2007). Stable Isotope-Based Paleoaltimetry. *Annual Review of Earth and Planetary Sciences*, *35*(1), 463–508. https://doi.org/10.1146/annurev.earth.35.031306.140155

Searle, M. P., Roberts, N. M. W., Chung, S.-L., Lee, Y.-H., Cook, K. L., Elliott, J. R., et al. (2016). Age and anatomy of the Gongga Shan batholith, eastern Tibetan Plateau, and its relationship to the active Xianshui-he fault. *Geosphere*, *12*(3), 948–970. https://doi.org/10.1130/ges01244.1

Spicer, R. A., Harris, N. B. W., Widdowson, M., Herman, A. B., Guo, S., Valdes, P. J., et al. (2003). Constant elevation of southern Tibet over the past 15 million years. *Nature*, *421*(6923), 622–624. https://doi.org/10.1038/nature01356

Su, T., Farnsworth, A., Spicer, R. A., & Huang, J. (2019). No high Tibetan Plateau until the Neogene. *SCIENCE ADVANCES*, 9.

Sun, B., Wang, Y.-F., Li, C.-S., Yang, J., Li, J.-F., Li, Y.-L., et al. (2015). Early Miocene elevation in northern Tibet estimated by palaeobotanical evidence. *Sci Rep*, *5*, 10379. https://doi.org/10.1038/srep10379

Sun, G.-Y., Hu, X.-M., Zhu, D.-C., Hong, W.-T., Wang, J.-G., & Wang, Q. (2015). Thickened juvenile lower crust-derived ~90Ma adakitic rocks in the central Lhasa terrane, Tibet. *Lithos*, *224–225*, 225–239. https://doi.org/10.1016/j.lithos.2015.03.010

Tapponnier, P., Zhiqin, X., Roger, F., Meyer, B., Arnaud, N., Wittlinger, G., & Jingsui, Y. (2001). Oblique Stepwise Rise and Growth of the Tibet Plateau. *Science*, *294*(5547), 1671–1677. https://doi.org/10.1126/science.105978

Taylor, M., & Yin, A. (2009). Active structures of the Himalayan-Tibetan orogen and their relationships to earthquake distribution, contemporary strain field, and Cenozoic volcanism. *Geosphere*, *5*, 199–214. https://doi.org/doi.org/10.1130/GES00217.1

Wang, C., Zhao, X., Liu, Z., Lippert, P. C., Graham, S. A., Coe, R. S., et al. (2008). Constraints on the early uplift history of the Tibetan Plateau. *Proceedings of the National Academy of Sciences*, *105*(13), 4987–4992. https://doi.org/10.1073/pnas.0703595105

Wang, J.-G., Hu, X., Garzanti, E., BouDagher-Fadel, M. K., Liu, Z.-C., Li, J., & Wu, F.-Y. (2020). From extension to tectonic inversion: Mid-Cretaceous onset of Andean-type orogeny in the Lhasa block and early topographic growth of Tibet. *GSA Bulletin*. https://doi.org/10.1130/B35314.1

Xu, Q., Ding, L., Zhang, L., Cai, F., Lai, Q., Yang, D., & Liu-Zeng, J. (2013). Paleogene high elevations in the Qiangtang Terrane, central Tibetan Plateau. *Earth and Planetary Science Letters*, *362*, 31–42. https://doi.org/10.1016/j.epsl.2012.11.058

Xu, Q., Ding, L., Hetzel, R., Yue, Y., & Rades, E. F. (2015). Low elevation of the northern Lhasa terrane in the Eocene: Implications for relief development in south Tibet. *Terra Nova*, *27*(6), 458–466. https://doi.org/10.1111/ter.12180

Yi, J.-K., Wang, Q., Zhu, D.-C., Li, S.-M., Liu, S.-A., Wang, R., et al. (2018). Westward-younging high-Mg adakitic magmatism in central Tibet: Record of a westward-migrating lithospheric foundering beneath the Lhasa–Qiangtang collision zone during the Late Cretaceous. *Lithos*, *316–317*, 92–103. https://doi.org/10.1016/j.lithos.2018.07.001

Yin, A., Harrison, T. M., Murphy, M. A., Grove, M., Nie, S., Ryerson, F. J., et al. (1999). Tertiary deformation history of southeastern and southwestern Tibet during the Indo-Asian collision. *GSA Bulletin*, *111*(11), 1644–1664. https://doi.org/10.1130/0016-7606(1999)111<1644:TDHOSA>2.3.CO;2

Zhao, Z., Bons, P. D., Stübner, K., Wang, G.-H., & Ehlers, T. A. (2017). Early Cretaceous exhumation of the Qiangtang Terrane during collision with the Lhasa Terrane, Central Tibet. *Terra Nova*, *29*(6), 382–391. https://doi.org/10.1111/ter.12298

Zhao, Z., Bons, P. D., Li, C., Wang, G. H., Ma, X. X., & Li, G. W. (2020). The Cretaceous crustal shortening and thickening of the South Qiangtang Terrane and implications for proto-Tibetan Plateau formation. *Gondwana Research*, *78*, 141–155. https://doi.org/10.1016/j.gr.2019.09.003

Zheng, Y., & Wu, F. (2018). The timing of continental collision between India and Asia. *Science Bulletin*, *63*(24), 1649–1654. https://doi.org/10.1016/j.scib.2018.11.022

Zhu, D.-C., Wang, Q., Cawood, P. A., Zhao, Z.-D., & Mo, X.-X. (2017). Raising the Gangdese Mountains in southern Tibet. *Journal of Geophysical Research: Solid Earth*, *122*(1), 214–223. https://doi.org/10.1002/2016jb013508

Zhu, D.-C., Wang, Q., Chung, S.-L., Cawood, P. A., & Zhao, Z.-D. (2019). Gangdese magmatism in southern Tibet and India–Asia convergence since 120 Ma. *Geological Society, London, Special Publications*, *483*(1), 583–604. https://doi.org/10.1144/SP483.14